



# Influencing mechanism of Zn interlayer addition on hook defects of friction stir spot welded Mg–Al–Zn alloy joints



R.Z. Xu<sup>a,b</sup>, D.R. Ni<sup>a</sup>, Q. Yang<sup>a</sup>, C.Z. Liu<sup>b</sup>, Z.Y. Ma<sup>a,\*</sup>

<sup>a</sup> Shenyang National Laboratory for Materials Science, Institute of Metal Research, Chinese Academy of Sciences, 72 Wenhua Road, Shenyang 110016, China

<sup>b</sup> College of Material Science and Engineering, Shenyang Aerospace University, 37 Daoyi South Street, Shenyang 110136, China

## ARTICLE INFO

### Article history:

Received 11 October 2014

Accepted 23 December 2014

Available online 5 January 2015

### Keywords:

Friction stir spot welding

Magnesium alloys

Hook defects

Interlayer

Alloying

## ABSTRACT

2.4 mm thick Mg–Al–Zn alloy sheets were friction stir spot welded (FSSW) without and with the addition of 0.1 mm thick Zn interlayer. The influence of interlayer addition on the microstructural features and mechanical properties of FSSW joints was investigated by optical microscope, scanning electron microscope, transmission electron microscope, X-ray diffraction and tensile testing. The results show that the addition of Zn interlayer resulted in complex alloying reactions between Mg substrate and Zn interlayer, forming a bonded zone composed of  $\alpha$ -Mg, ( $\alpha$ -Mg + MgZn) eutectoid structure and a mixture of Mg<sub>4</sub>Zn<sub>7</sub> and unreacted Zn, thereby increasing the area of bonded zone and reducing the hook defects. This results in a significant increase in tensile–shear load from 2.4 kN to about 4 kN.

© 2015 Elsevier Ltd. All rights reserved.

## 1. Introduction

Magnesium alloys are excellent candidates for lightweight structural applications in the automotive and aerospace industries due to their low density, high specific strength and acceptable ductility [1]. However, they are difficult to weld by conventional fusion welding techniques due to the active behavior of Mg. This problem could be solved by friction stir welding (FSW) that is a solid-state joining technique [2–5].

In FSW, friction stir lap welding (FSLW) is the most common weld configuration for automotive and aerospace industries [6,7]. Especially, friction stir spot welding (FSSW) is one of the most important FSLW [8,9]. However, a characteristic feature of FSSW is the formation of a geometrical defect originating at the interface between the two welded sheets, called as hook defect [10]. The presence of hook defects in the weld zone decreases the integrity of the bonded region and thus significantly reduces the weld strength since the failure (crack propagation) occurs along the hook line.

For FSSW of Mg alloys, the effect of hook defects on the joint load has attracted much attention in recent years [11]. Many studies focused on changing the dimensions and curvatures of the hook by the optimization of process condition and tool geometry. However, the formation of hook defects could not be completely

avoided in the FSSW joints [11–13]. In order to reduce the effect of the hook defects and enhance the load of joints, some hybrid FSSW methods were applied to the Mg alloys, such as bonding-FSSW [14] and FSSW with a heating process [15].

For the bonding-FSSW of AZ31 Mg alloy, the area of bonded zone of joints was increased by adhesives, so the load of joints was improved [14]. However, the aging and poor high-temperature performance of adhesives were the main drawbacks for this process. For the FSSW AZ31 Mg alloy with a heating process, the area of the bonded zone was increased remarkably by heating the joints in the FSSW process [15]. However, the troublesome operation limited its wide application. In fact, above two hybrid technologies increased only the area of bonded zone, but could not avoid the appearance of hook defects. Therefore, new processes are still needed for reducing the hook defects of FSSW Mg alloy joints.

According to the Mg–Zn phase diagram [16], Zn could react with Mg at a low temperature, forming the Mg–Zn intermetallics. Therefore, the idea of reducing the hook defects by the alloying reaction was proposed with Zn as the alloying element. Prior to FSSW, Zn interlayer was added at the interface between two welded Mg sheets with the aim to promote the bonding of facing surface of Mg sheets and reduce the formation of hook defects, thereby improving the load of FSSW joints.

In this study, 2.4 mm thick AZ31 and AZ80 sheets were FSSWed with the combinations of AZ31–AZ31, AZ31–AZ80 and AZ80–AZ80 and the influencing mechanism of Zn interlayer addition on the hook defects of FSSW joints was in detail investigated.

\* Corresponding author. Tel./fax: +86 24 83978908.

E-mail address: [zyrna@imr.ac.cn](mailto:zyrna@imr.ac.cn) (Z.Y. Ma).

## 2. Experimental details

The substrate materials used in the present study were 2.4 mm thick sheets of hot-rolled AZ31 Mg alloy with a composition of Mg–3.02Al–0.82Zn–0.30Mn–0.01Si (wt.%) and hot-rolled AZ80 Mg alloy with a composition of Mg–8.00Al–0.33Zn–0.25Mn–0.036Si (wt.%). The schematic of FSSW without and with the addition of Zn interlayer is shown in Fig. 1. Before welding, the sheets were ground by the 800<sup>#</sup> SiC paper, and then cleaned by acetone. For the FSSW with the Zn interlayer, 0.2 mm thick pure Zn interlayer was added between two welded Mg sheets prior to the welding operation. All the FSSW operations with and without the interlayer were conducted at a tool rotational rate of 3000 rpm and a plunge rate of 2.5 mm/s using a tool with a concave shoulder 10 mm in diameter and a threaded cylindrical pin 4 mm in diameter and 3.8 mm in length. The tool withdrawing rate was 30 mm/s at the end of each spot welding operation and the dwell time was 5 s.

The temperature profile of the interface zone during FSSW was measured by a K-type thermocouple 0.5 mm in diameter. A cylindrical hole 0.8 mm in diameter and 2.3 mm in length was machined in the bottom sheet of Mg alloy and a thermocouple was fastened at the top of the hole by high temperature glue. The schematic of temperature measurement is shown in Fig. 1c.

Specimens for microstructure examinations were sectioned through the center of the welded joints and parallel to the loading direction. After being mechanically ground and polished, the specimens were etched with an etching reagent consisting of 4.2 g picric acid, 10 ml acetic acid, 10 ml H<sub>2</sub>O and 70 ml ethanol. Microstructures were examined by optical microscope (OM), scanning electron microscope (SEM, LEO Supra 35) with the energy dispersive spectrometer (EDS) and transmission electron microscope (TEM, Tecnai F20). The material of Mg–Zn interface zone in FSSW AZ31 joints was prepared into powders and then subjected to X-ray diffraction (XRD) analysis using Cu K $\alpha$  radiation.

The lap-shear specimens with a length of 100 mm, a width of 30 mm and a 30  $\times$  30 mm overlap area were electrical discharge machined from the FSSW joints. The lap-shear tensile tests were conducted using a Zwick/Roell Z050 tester at a tensile speed of 1 mm/min. The rolling direction was perpendicular to the shear tensile testing direction. The property values for each condition were calculated by averaging three test results. The fracture characteristics were examined using SEM.

## 3. Results and discussion

### 3.1. Microstructure of FSSW Mg alloy joints without the addition of Zn interlayer

Fig. 2a–c shows the typical cross-section photographs of the FSSW AZ31–AZ31, AZ31–AZ80 and AZ80–AZ80 joints without the addition of Zn interlayer, respectively. The hook defects were all detected in three spot joints, which further proved that the hook defects were easy to form in the FSSW Mg alloy joints. The average height of hook of three joints is 0.62, 0.68 and 0.72 mm, respectively.

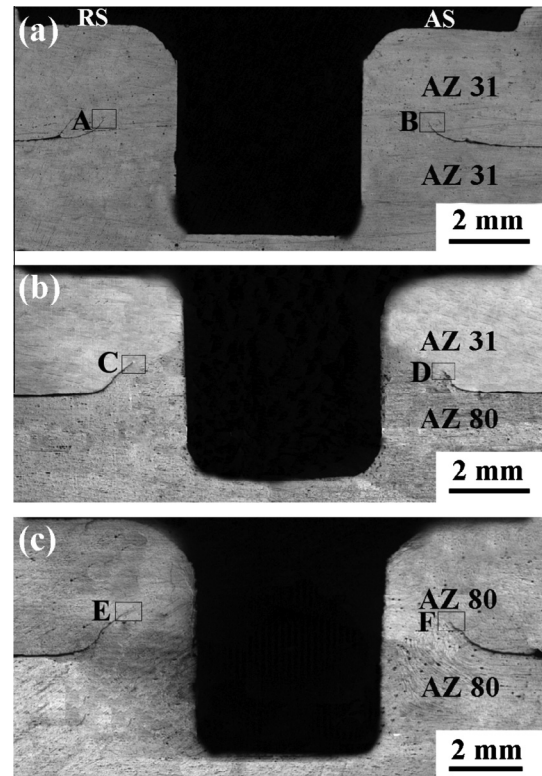


Fig. 2. Typical cross-section photographs of joints without the addition of Zn interlayer: (a) AZ31–AZ31, (b) AZ31–AZ80 and (c) AZ80–AZ80.

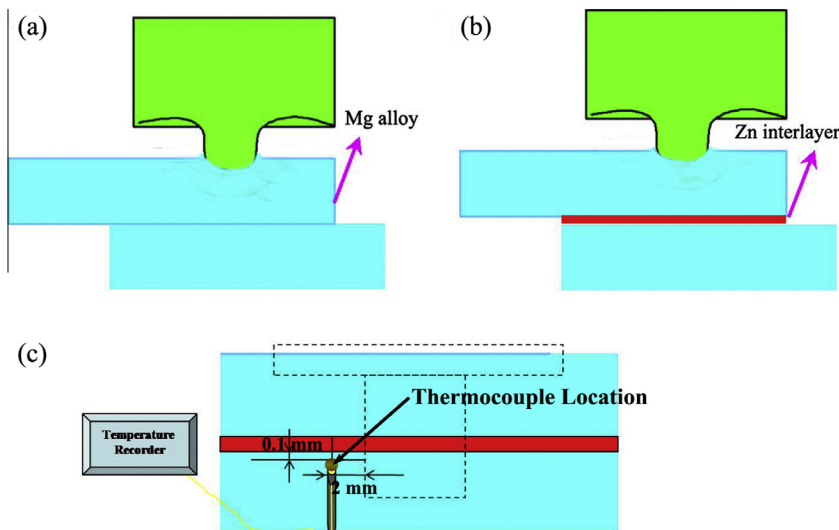


Fig. 1. Schematics of FSSW (a) without and (b) with the addition of Zn interlayer and (c) the position of temperature measurement.

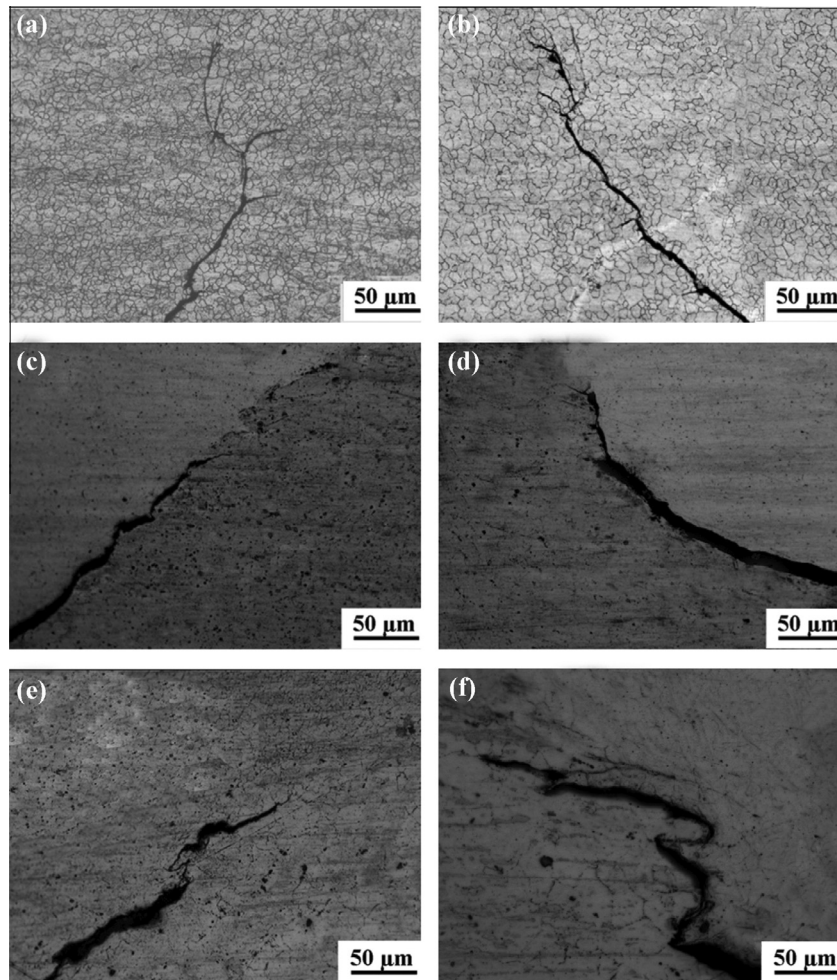


Fig. 3. Magnified micrographs of regions (a) A, (b) B, (c) C, (d) D, (e) E and (f) F in Fig. 2.

Fig. 3a–f shows the magnified micrographs of regions A–F in Fig. 2, respectively. The hook defects on both the advancing side and the retreating side extended upward towards the keyhole periphery, which was attributed to the material flow characteristics during FSSW [6,8]. The previous studies proved that the hook originated from the faying surface of the two sheets due to the incomplete break-up of the Mg oxide film [17]. When using a threaded pin for FSSW, the heated and softened material underneath the shoulder first moved toward the pin root and then moved along the pin surface downwards as a result of the dragging force of the rotating threads. Once the material arrived at the pin tip, it was forced upward [18,19], which resulted in the upward bending of the work-piece interface. At last, the hook defects were formed.

### 3.2. The effect of adding Zn interlayer on the microstructure of FSSW Mg alloy joints

Fig. 4a–c shows the typical cross-section photographs of the FSSW AZ31–AZ31, AZ31–AZ80 and AZ80–AZ80 joints with the addition of Zn interlayer, respectively. It is obvious that the hook defects were reduced in all the joints. Fig. 5a–c shows the magnified micrographs of regions A, B and C in Fig. 4, respectively. The reaction layer formed between Mg substrate and Zn interlayer replaced unbonded zone in the joints without the Zn interlayer (Fig. 3).

In order to reveal the microstructure and phase composition at the interface between Mg substrate and Zn interlayer, the FSSW

AZ31–AZ31 joint with the addition of Zn interlayer was further investigated. Fig. 6 shows the SEM microstructure of the interface between Mg substrate and Zn interlayer. It could be found that an obvious transition zone was formed at the interface due to the diffusion reaction of Mg substrate and Zn interlayer. The transition zone could be divided into zones I, II and III from the AZ31 substrate to the Zn interlayer according to the different microstructures. The XRD analysis indicated that the whole transition zone was composed of  $\alpha$ -Mg, MgZn,  $Mg_4Zn_7$  and remnant Zn (Fig. 7).

Fig. 8 shows the TEM images of typical zones from the Mg substrate to the Zn interlayer. The element contents of regions A to E in Fig. 8a–c determined by EDS are shown in Table 1. Fig. 8a shows the microstructure of zone I adjacent to the Mg side (Fig. 6). It was indicated that the structure marked with A was the  $\alpha$ -Mg phase with a few small Mg–Zn precipitates. Fig. 8b shows the microstructure of zone II (Fig. 6). The refined eutectoid structure was detected in this zone. According to the EDS results, XRD analysis and Mg–Zn phase diagram [16], zone II was composed of the ( $\alpha$ -Mg + MgZn) eutectoid structure. The electron micro-diffraction patterns from the gray phase in Fig. 8b further proved that the precipitated phase was MgZn. Fig. 8c and d shows the TEM microstructure of zone III in Fig. 6 and its electron micro-diffraction pattern, respectively. It could be determined that this zone was the mixture of  $Mg_4Zn_7$  (also known as  $Mg_2Zn_3$ ) [20] and remnant Zn.

During the FSSW process of Mg alloys, the temperature could reach above 400 °C due to the thermo-mechanical action of stir

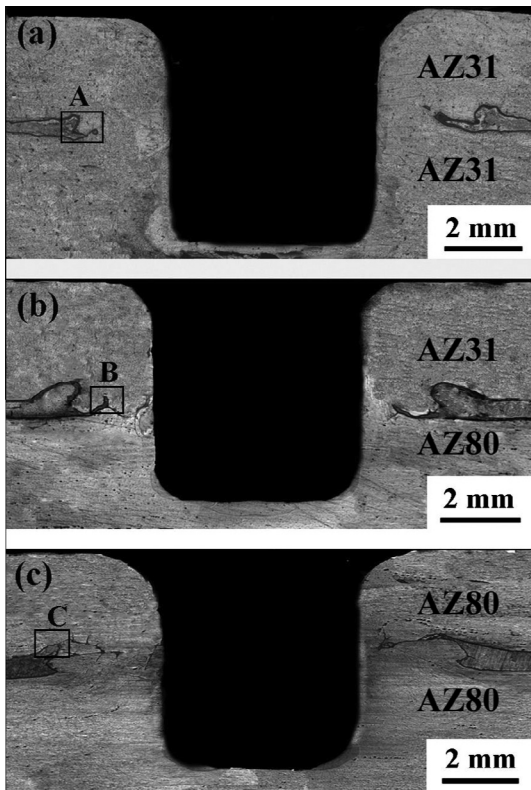


Fig. 4. Typical cross-section photographs of joints with the addition of Zn interlayer: (a) AZ31–AZ31, (b) AZ31–AZ80 and (c) AZ80–AZ80.

tool (Fig. 9), which is sufficient to promote the diffusion reaction between Mg substrate and Zn interlayer. The formation of intermetallic compounds in the FSSW process could be understood based on the Mg–Zn binary phase diagram [16].

In zone I, the content of Mg was much higher than that of Zn as shown in Table 1, only a little of Zn interlayer could diffuse into the

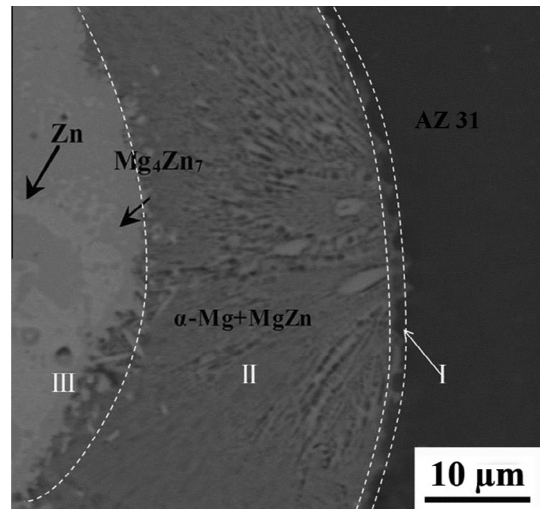


Fig. 6. SEM microstructure of the interface between Mg substrate and Zn interlayer.

Mg substrate in FSSW. During the cooling period, the transformation occurred:  $L \rightarrow \alpha\text{-Mg}$ . With the further decrease of temperature, a few small MgZn phases precipitated from the  $\alpha\text{-Mg}$  as shown in Fig. 8a. At last, the structure was composed of  $\alpha\text{-Mg}$  with a few small MgZn phases.

In zone II, the AZ31 substrate was dissolved into the molten Zn interlayer in the FSSW process. As a result, in this zone, the relative content of Mg element increased and the content of Zn element decreased. With the decrease of the temperature,  $\text{Mg}_7\text{Zn}_3$  phase was formed by a eutectic reaction at  $340^\circ\text{C}$ :  $L \rightarrow \alpha\text{-Mg} + \text{Mg}_7\text{Zn}_3$ . Then, with the further decrease of the temperature, some MgZn phases were eventually generated by a eutectoid reaction at  $325^\circ\text{C}$ :  $\text{Mg}_7\text{Zn}_3 \rightarrow \alpha\text{-Mg} + \text{MgZn}$ . At last, eutectoid microstructure composed of  $\alpha\text{-Mg}$  and MgZn was formed as shown in Figs. 6a and 8b.

In zone III, the content of Zn was much higher than that of Mg as shown in Table 1, so a part of Zn could react with the Mg that diffused into the interlayer to form  $\text{Mg}_4\text{Zn}_7$ :  $\alpha\text{-Mg} + \text{Zn} \rightarrow \text{Mg}_4\text{Zn}_7$ .

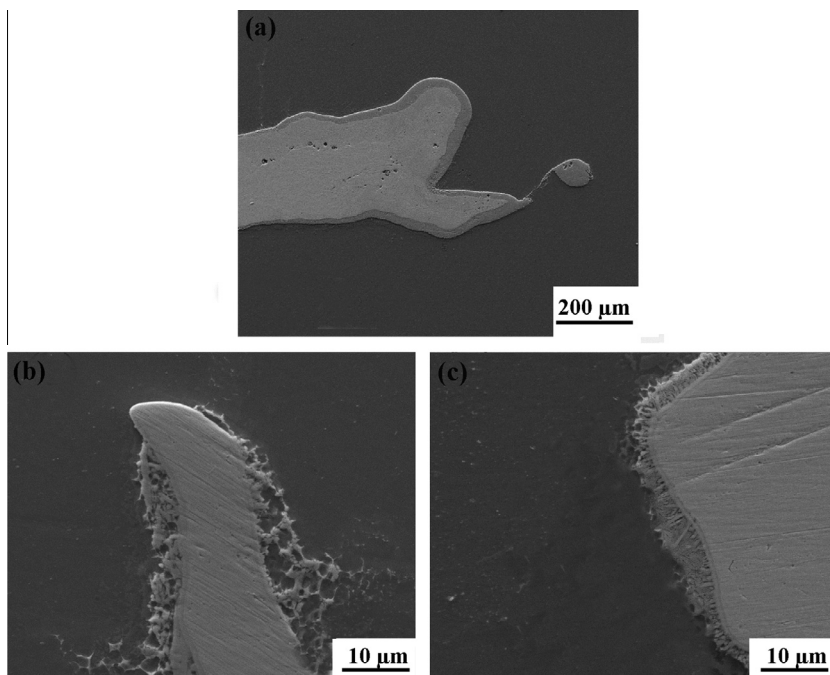


Fig. 5. Magnified micrographs of regions (a) A, (b) B and (c) C in Fig. 4.

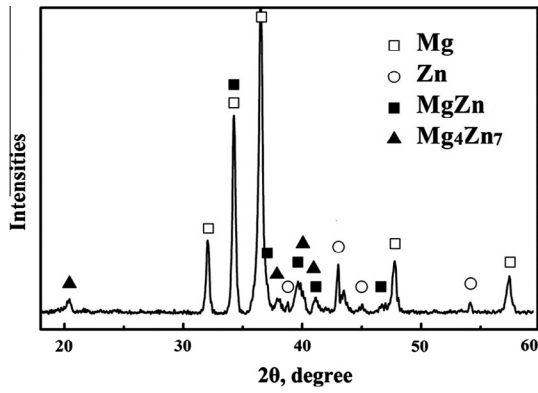


Fig. 7. XRD pattern of the interface between Mg substrate and Zn interlayer.

The formed  $Mg_4Zn_7$  could not decompose in time in this zone during the rapid cooling period. In addition, the unreacted Zn remained in this zone after FSSW. Therefore, zone III was composed of a mixture of  $Mg_4Zn_7$  and residual Zn (Fig. 8c and d).

To sum up, alloying process between Zn interlayer and Mg substrate during FSSW involved in a complex phase transformation reaction, resulting in the formation of a variety of Mg–Zn intermetallic compounds.

3.3. The effect of adding Zn interlayer on the properties of FSSW Mg alloy joints

In order to demonstrate the beneficial effect of Zn interlayer, tensile shear data for various FSSW Mg alloy joints prepared under a variety of FSSW conditions (including hybrid FSSW) in recent

Table 1

The element contents of regions A to E in Fig. 8a–c determined by EDS.

| Region | Element (at.%) |      | Possible phases                    |
|--------|----------------|------|------------------------------------|
|        | Mg             | Zn   |                                    |
| A      | 93.4           | 6.6  | $\alpha$ -Mg with a few small MgZn |
| B      | 92.3           | 7.7  | $\alpha$ -Mg with a few small MgZn |
| C      | 51.6           | 48.4 | MgZn                               |
| D      | 35.7           | 64.3 | $Mg_4Zn_7$                         |
| E      | 99.8           | 0.02 | Zn                                 |

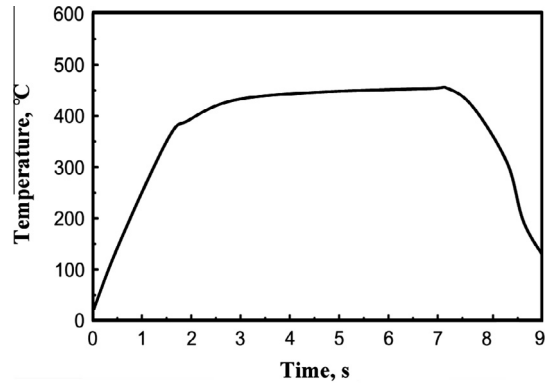


Fig. 9. Temperature change at distances of 2.0 mm from the periphery of the rotating pin.

years are summarized in Table 2 [12,14,15,21–24]. It is evident that, many factors, such as sheet thickness, stir tool and hybrid welding, could affect the strength of joints. It is noted that the

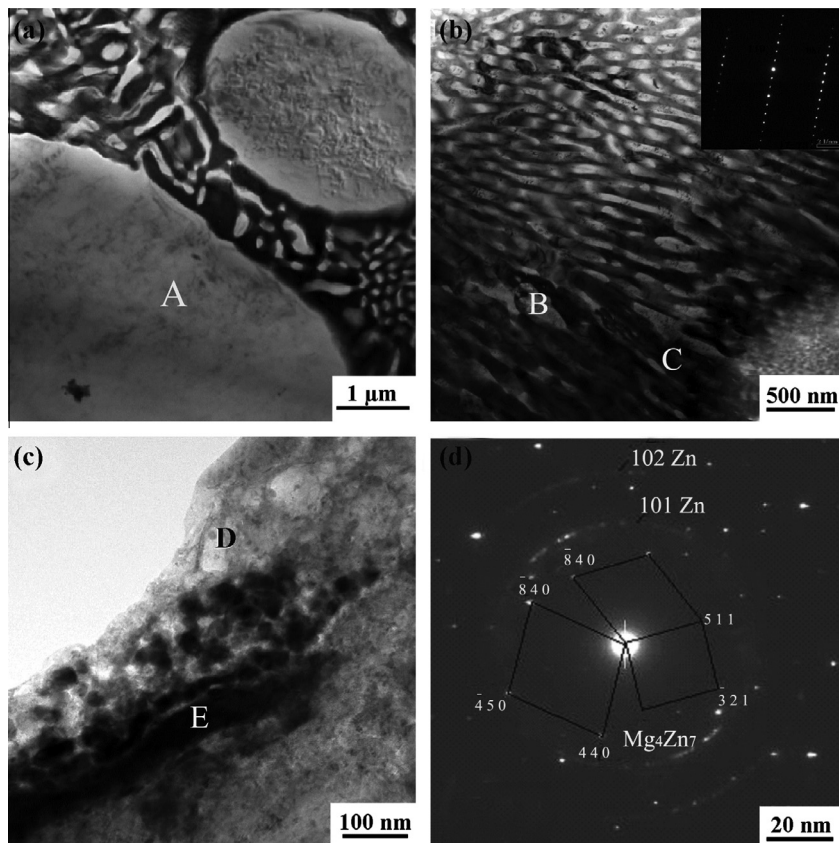
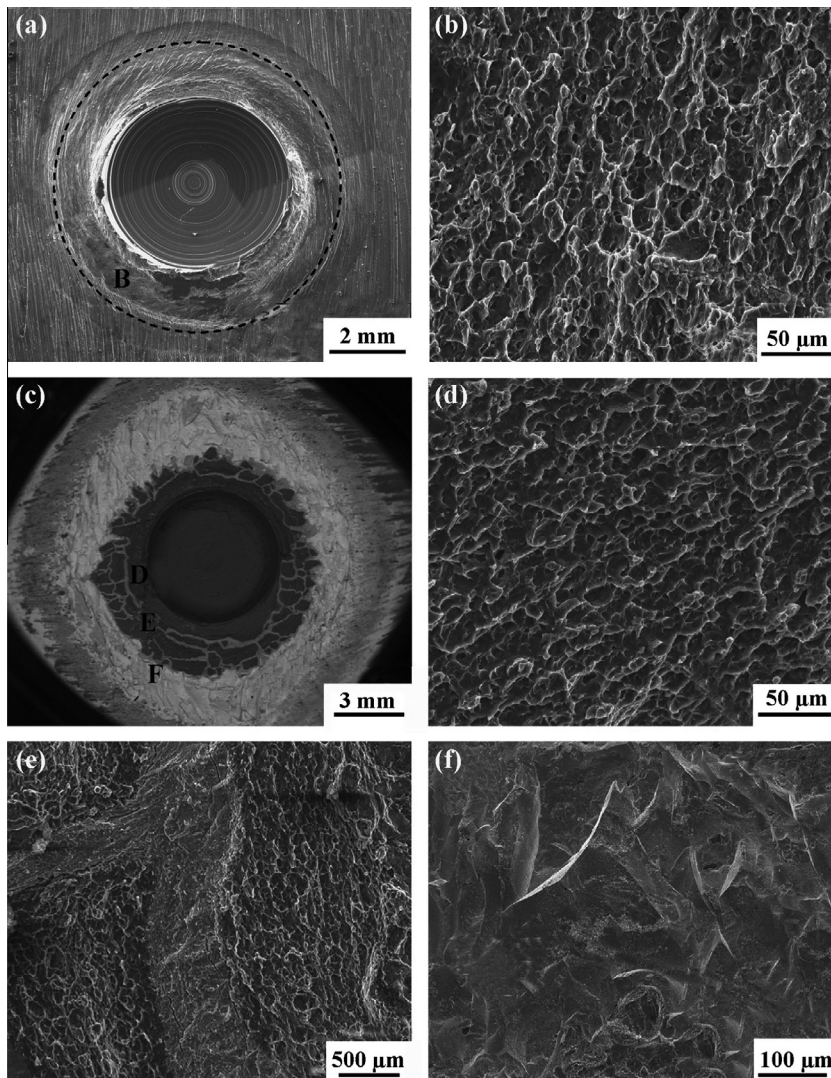


Fig. 8. TEM images of typical transition zones from Mg alloy substrate to Zn interlayer: (a) zone I, (b) zone II and electron micro-diffraction pattern of MgZn ( $\bar{7}\bar{7}5$ ), (c) zone III and (d) electron micro-diffraction pattern ( $Mg_4Zn_7$ : pdf-85-1260).

**Table 2**

A summary of tensile shear data for various FSSW Mg alloy joints prepared under a variety of FSSW conditions (10 mm shoulder diameter).

| Mg alloy FSSW joint | Sheet thickness (mm) | Pin, or Hybrid process                                    | Maximum load (kN) | Refs.        |
|---------------------|----------------------|---|-------------------|--------------|
| AZ31–AZ31           | 1.5                  | Cylindrical pin with M4 thread                            | 2.2               | [12]         |
| AZ31–AZ31           | 1.5                  | Three-flat/0.5 mm/M4 thread                               | 2.0               | [12]         |
| AZ31–AZ31           | 1.5                  | Three-flat/0.7 mm/M4 thread                               | 2.6               | [12]         |
| AZ31–AZ31           | 1.5                  | Three-flat/no thread cylindrical pin                      | 2.5               | [12]         |
| AZ31–AZ31           | 1.6                  | Cylindrical pin with M4 thread                            | 2.9               | [21]         |
| AZ31–AZ31           | 2.5                  | Cylindrical pin with M4 thread                            | 1.5               | [22]         |
| AZ61–AZ61           | 2.5                  | Cylindrical pin with M4 thread                            | 1.8               | [22]         |
| AZ31–AZ31           | 1.5                  | Cylindrical pin with M4 thread                            | 2.3               | [23]         |
| AZ31–AZ31           | 1.5                  | Three-flat/M4 thread                                      | 2.5               | [23]         |
| AM60–AM60           | 1.5                  | Cylindrical pin with M4 thread                            | 1.4               | [23]         |
| AM60–AM60           | 1.5                  | Three-flat/M4 thread                                      | 2.1               | [23]         |
| AZ91–AZ31           | 1.5                  | Cylindrical pin with M4 thread                            | 1.4               | [24]         |
| AZ91–AZ31           | 1.5                  | Three-flat/0.7 mm/M4 thread                               | 1.3               | [24]         |
| AZ91–AZ31           | 1.5                  | Three-flat/no thread                                      | 1.1               | [24]         |
| AZ31–AZ31           | 2.4                  | Cylindrical pin/FSSW, FSSW + Heat process                 | 0.7, 1.5          | [15]         |
| AZ31–AZ31           | 3.0                  | Cylindrical pin with M4 thread/FSSW, Bonding + FSSW       | 3.0, 3.6          | [14]         |
| AZ31–AZ31           | 2.4                  | Cylindrical pin with M4 thread/FSSW, FSSW + Zn Interlayer | 2.4, 4.1          | Present work |
| AZ80–AZ80           | 2.4                  | Cylindrical pin with M4 thread/FSSW, FSSW + Zn Interlayer | 1.9, 4.0          | Present work |
| AZ31–AZ80           | 2.4                  | Cylindrical pin with M4 thread/FSSW, FSSW + Zn Interlayer | 1.8, 3.9          | Present work |



**Fig. 10.** SEM images of fracture surfaces: (a) macrostructure and (b) microstructure of joints without addition of Zn interlayer; (c) macrostructure and microstructure of (d) zone D, (e) zone E and (f) zone F of joints with addition of Zn interlayer.

strength of FSSW Mg alloy joints with the addition of Zn interlayer was superior to that of other joints. In other words, the addition of

Zn interlayer could improve significantly the strength of FSSW Mg alloy joints.

Fig. 10a and b shows the SEM macrographs of the fracture surfaces of the AZ31–AZ31 joints without the addition of Zn interlayer and the magnified micrograph of region B, respectively. The fracture surface consisting of tear ridges, dimples and cleavage facets exhibited a quasi-cleavage crack feature. Fig. 10c shows the SEM macrograph of the fracture surface of the AZ31–AZ31 joints with the addition of Zn interlayer. It can be found that the fracture surface could be divided into three types of regions, i.e., regions D, E and F. In region D, similar to the joint without the Zn interlayer, fracture exhibited quasi-cleavage crack feature (Fig. 10d). In region E, some stripes formed by the reaction of Mg and Zn elements were detected, but the fracture also exhibited the characteristic of cleavage fracture (Fig. 10e). Compared to the joint without the Zn interlayer, region F was the newly-formed zone due to the brazing reaction between Zn interlayer and Mg substrate for the joint with the Zn interlayer. The fracture of region F was brittle as shown in Fig. 10f. However, the existence of region F enhanced significantly the area of bonded zone, which was beneficial to the increase of the joint load.

Based on above analysis, after the addition of Zn interlayer, the significant increase of load was attributed to the diffusion reaction between Mg substrate and Zn interlayer for the FSSW Mg alloy joints. First, the Zn interlayer could react with the Mg substrate under the thermo-mechanical action of stir tool to promote the joining of upper and bottom sheets of Mg alloy. So the addition of Zn interlayer reduced the hook defects of joints. Second, the formation of transition zone between Zn interlayer and Mg substrate could increase the area of the bonded zone, thereby increasing the load of joints.

#### 4. Conclusions

In summary, adding Zn interlayer could lower the reaction temperature of interface and promote the diffusion reaction between Zn interlayer and Mg substrate, forming a bonded zone composed of  $\alpha$ -Mg, ( $\alpha$ -Mg + MgZn) eutectoid structure and a mixture of Mg<sub>4</sub>Zn<sub>7</sub> and unreacted Zn. As a result, the tensile–shear load of the joints was significantly improved due to the decrease of hook defects as well as the increase of the area of bonded zone. The maximum load could reach about 4 kN, which is superior to that of other FSSW methods.

#### Acknowledgements

This study was supported by the National R&D Program of China under Grant No. 2011BAE22B05, and the National Natural Science Foundation of China under Grant Nos. 51371179 and 51331008.

#### References

- [1] Patel VK, Bhole SD, Chen DL. Influence of ultrasonic spot welding on microstructure in a magnesium alloy. *Scripta Mater* 2011;65:911–4.
- [2] Afrin N, Chen DL, Cao X, Jahazi M. Strain hardening behavior of a friction stir welded magnesium alloy. *Scripta Mater* 2007;57:1004–7.
- [3] Yang J, Ni DR, Wang D, Xiao BL, Ma ZY. Friction stir welding of as-extruded Mg–Al–Zn alloy with higher Al content. Part I: Formation of banded and line structures. *Mater Charact* 2014;96:142–50.
- [4] Yang J, Ni DR, Wang D, Xiao BL, Ma ZY. Friction stir welding of as-extruded Mg–Al–Zn alloy with higher Al content. Part II: Influence of precipitates. *Mater Charact* 2014;96:135–41.
- [5] Padmanaban G, Balasubramanian V. Fatigue performance of pulsed current gas tungsten arc, friction stir and laser beam welded AZ31B magnesium alloy joints. *Mater Des* 2010;31:3724–32.
- [6] Yang Q, Li X, Chen K, Shi YJ. Effect of tool geometry and process condition on static strength of a magnesium friction stir lap linear weld. *Mater Sci Eng A* 2011;528:2463–78.
- [7] Cao X, Jahazi M. Effect of tool rotational speed and probe length on lap joint quality of a friction stir welded magnesium alloy. *Mater Des* 2011;32:1–11.
- [8] Wei Y, Li JL, Xiong JT, Huang F, Zhang FS. Microstructures and mechanical properties of magnesium alloy and stainless steel weld-joint made by friction stir lap welding. *Mater Des* 2012;33:111–4.
- [9] Chen YC, Nakata K. Effect of tool geometry on microstructure and mechanical properties of friction stir lap welded magnesium alloy and steel. *Mater Des* 2009;30:3913–9.
- [10] Yuan W, Mishra RS, Webb S, Chen YL, Carlson B, Herling DR, et al. Effect of tool design and process parameters on properties of Al alloy 6016 friction stir spot welds. *J Mater Process Technol* 2011;211:972–7.
- [11] Yin YH, Sun N, North TH, Hu SS. Hook formation and mechanical properties in AZ31 friction stir spot welds. *J Mater Process Technol* 2010;210:2062–70.
- [12] Yin YH, Sun N, North TH, Hu SS. Influence of tool design on mechanical properties of AZ31 friction stir spot welds. *Sci Technol Weld Join* 2010;15:81–6.
- [13] Yamamoto M, Gerlich A, North TH, Shinozaki K. Cracking in the stir zones of Mg-alloy friction stir spot welds. *J Mater Sci* 2007;42:7657–66.
- [14] Ni YQ. Study on the bonding-friction stir spot hybrid welding procedure of AZ31 Mg alloy. Dalian: Dalian Jiaotong University; 2012.
- [15] Shen J, Min D, Wang D. Effects of heating process on the microstructures and tensile properties of friction stir spot welded AZ31 magnesium alloy plates. *Mater Des* 2011;32:5033–7.
- [16] Clark JB, Zabdyr L, Moser Z. In: Nayebhashemi AA, Clark JB, editors. Phase diagrams of binary magnesium alloys. Metals PARK, OH: ASM International; 1988. p. p353.
- [17] Yuan W, Mishra RS, Carlson B, Verma R, Mishra RK. Material flow and microstructural evolution during friction stir spot welding of AZ31 magnesium alloy. *Mater Sci Eng A* 2012;543:200–9.
- [18] Su P, Gerlich A, North TH, Bendzsak GJ. Material flow during friction stir spot welding. *Sci Technol Weld Join* 2006;11:61–6.
- [19] Gerlich A, Su P, Yamamoto M, North TH. Material flow and intermixing during dissimilar friction stir welding. *Sci Technol Weld Join* 2008;13:254–64.
- [20] Gao X, Nie JF. Structure and thermal stability of primary intermetallic particles in an Mg–Zn casting alloy. *Scripta Mater* 2007;57:655–8.
- [21] Horie S, Shinozaki K, Yamamoto M, Kadoi K, Nakashin H, North TH. Effects of tool geometry and process conditions on material flow and strength of friction stir spot welded joints. *Trans JWRI* 2010;39:28–36.
- [22] Wang D, Shen J, Wang LZ. Effects of the types of overlap on the mechanical properties of FSSW welded AZ series magnesium alloy joints. *Inter J Miner Metall Mate* 2012;19:231–5.
- [23] Yin YH, Ikuta A, North TH. Microstructural features and mechanical properties of AM60 and AZ31 friction stir spot welds. *Mater Des* 2010;31:4764–76.
- [24] Yin YH, Sun N, North TH, Hu SS. Microstructures and mechanical properties in dissimilar AZ91/AZ31 spot welds. *Mater Charact* 2010;61:1018–28.